Eur. Phys. J. D **33**, 99–112 (2005)
DOI: 10.1140/epjd/e2005-00011-3

THE EUROPEAN PHYSICAL JOURNAL D

Lithium atom interferometer using laser diffraction: description and experiments

A. Miffre, M. Jacquey, M. Büchner, G. Trénec, and J. Vigué[a]

Laboratoire Collisions Agrégats Réactivité, IRSAMC, Université Paul Sabatier and CNRS UMR 5589, 118 route de Narbonne, 31062 Toulouse Cedex, France

Received 25 October 2004
Published online 1st February 2005 –

Abstract. We have built and operated an atom interferometer of the Mach-Zehnder type. The atomic wave is a supersonic beam of lithium seeded in argon and the mirrors and beam-splitters for the atomic wave are based on elastic Bragg diffraction on laser standing waves at $\lambda = 671$ nm. We give here a detailed description of our experimental set-up and of the procedures used to align its components. We then present experimental signals, exhibiting atomic interference effects with a very high visibility, up to $84.5 \pm 1\%$. We describe a series of experiments testing the sensitivity of the fringe visibility to the main alignment defects and to the magnetic field gradient.

PACS. 39.20.+q Atom interferometry techniques – 03.75.Dg Atom and neutron interferometry – 32.80.Lg Mechanical effects of light on atoms, molecules, and ions

1 Introduction and brief historical overview

We have built a Mach-Zehnder atom interferometer, which gave its first signals in 2001 [1]. In this interferometer, the atomic wave is a supersonic beam of lithium seeded in argon, with a lithium de Broglie wavelength $\lambda_{\rm dB} = 54$ pm. Coherent atom manipulation is based on Bragg diffraction on quasi-resonant laser standing waves at a wavelength $\lambda_L \approx 671$ nm. We use elastic laser diffraction, which can be made with ordinary single frequency lasers, because this process has little sensitivity to the phase noise of the laser beams. However, the associated difficulty is that the output atomic beams differ only by their directions of propagation and not by their internal states. Therefore, such an interferometer must be operated with a highly collimated atomic beam resulting in a strongly reduced output atomic flux. Fortunately, the transmission of such a Bragg Mach-Zehnder interferometer is quite high and, thanks to an intense lithium beam and a very sensitive hot-wire atom detector, we obtain reasonably large signals. Moreover, we have been able to observe interference signals while using the diffraction orders $p = 1$, 2 and 3 and in the case of the first order, the signal exhibits an excellent fringe visibility $\mathcal{V} = 84.5 \pm 1\%$.

We may recall the development of atom interferometry since 1991, when several atom interferometers gave their first signals:

- a Young's double slit experiment by Carnal and Mlynek, with a supersonic beam of metastable helium [2];
- a Mach-Zehnder interferometer by Pritchard and co-workers using a thermal atomic beam of sodium and diffraction on material gratings [3];
- a Ramsey-Bordé interferometer by Helmcke and co-workers, with a thermal atomic beam of calcium, was used to demonstrate Sagnac effect with atomic waves [4];
- an atom interferometer using Raman diffraction by Kasevich and Chu, with cold sodium atoms, was used to make the first high sensitivity measurement of the local acceleration of gravity by atom interferometry [5].

This research field has been rapidly expanding since 1991 and an excellent overview of this field and of its applications can be found in the book "Atom interferometry" [6] published in 1997. Many types of atom interferometers have been developed and we limit the present review to the apparatuses in which the atomic paths are noticeably different, i.e. we will not discuss the interferometers, such as atomic clocks, in which the momentum transfer is very small. Moreover, we limit our review to interferometers operating with thermal atoms or molecules, quoting only the first publication for each interferometer. In addition to the interferometers built in 1991, we find: a magnesium atom interferometer by Ertmer and co-workers [7]; a calcium atom interferometer by Morinaga and co-workers [8]; an I_2 molecular interferometer by Bordé and co-workers [9]; a Na_2 molecular interferometer by Pritchard and co-workers [10]; a metastable argon interferometer of Zeilinger and co-workers [11]; a metastable neon interferometer by Siu Au Lee and co-workers [12]; a cesium atom interferometer gyroscope by Kasevich and co-workers [13]; a K_2 molecular interferometer by

[a] e-mail: jacques.vigue@irsamc.ups-tlse.fr

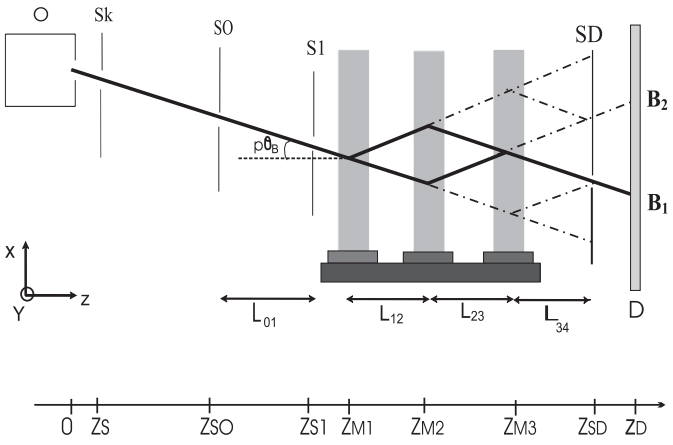

Fig. 1. Schematic drawing of our Mach-Zehnder interferometer (top view). The x-, y-, z-axis are represented and we give the distance z of each element to the nozzle. O: lithium oven; Sk: skimmer at $z_s = 20$ mm; S_0: first collimating slit at $z_{S0} = 485$ mm; S_1: second collimating slit at $z_{S1} = 1265$ mm; M_i, $i = 1{-}3$: mirrors for the laser standing waves at $z_{M1} = 1415$ mm, $z_{M2} = 2020$ mm and $z_{M3} = 2625$ mm; B_1 and B_2: complementary exit beams; S_D: detector slit with a tunable width at $z_{SD} = 3025$ mm; D: 760 μm wide rhenium hot wire of the Langmuir-Taylor detector at $z_D = 3375$ mm. We have also represented the main stray atomic beams produced by diffraction on the three gratings, assuming that only two diffraction orders, 0 and p are produced, as in the ideal Bragg regime.

Tiemann and co-workers [14], a helium atom and dimer interferometer by Toennies and co-workers [15], a large molecule interferometer by Zeilinger and co-workers [16]; a metastable hydrogen interferometer by Hänsch and co-workers [17].

In this paper, we recall the principles of Mach-Zehnder atom interferometers and of laser diffraction. Then, we explain our basic choices and we describe our set-up and its alignment procedures. We present a diffraction experiment, used to choose the parameters of the laser standing waves, and a set of interference signals recorded using the diffraction orders $p = 1, 2, 3$. We explain how we have optimized the fringe visibility by a systematic study of its variations with the main defects of the interferometer.

2 Mach-Zehnder atom interferometers: general properties and our design

2.1 General properties

A Mach-Zehnder grating interferometer is derived from the optical Mach-Zehnder interferometer by replacing the beam-splitters and mirrors by diffraction gratings. This interferometer was developed with X-rays [18] in 1965, with neutrons [19] in 1974 and with atoms [3,5] in 1991. Figure 1 presents a schematic drawing of the atom paths in such an interferometer. In the simplest approximation, the incident atomic wave is treated as a plane wave $\Psi(\mathbf{r}) = \exp[i\mathbf{k}\cdot\mathbf{r}]$ and diffraction of order p by grating G_j produces also a plane wave:

$$\Psi_d(\mathbf{r}) = \alpha_j(p)\exp\left[i\mathbf{k}\cdot\mathbf{r} + ip\mathbf{k}_{Gj}\cdot(\mathbf{r}-\mathbf{r}_j)\right]. \quad (1)$$

Conservation of energy and momentum must be fulfilled and equation (1) is exact only in the case of Bragg diffraction but, near this geometry, it is valid up to the first order in power of k_{Gj}/k. $\alpha_j(p)$ is the diffraction amplitude of order p by grating G_j. The wave vector $\mathbf{k}_{Gj}$ of grating G_j lies in the grating plane, perpendicular to its lines, with a modulus $k_{Gj} = 2\pi/a$ (a is the grating period, assumed to be the same for the three gratings). $\mathbf{r}_j$ measures the position of a reference point linked to grating G_j. As shown by equation (1), the phase of the diffracted beam depends rapidly on the position of the grating in its plane. The output beam labeled B_1 in Figure 1 results from the interference of two waves Ψ_u (following the upper path with the diffraction orders p, $-p$ and 0) and Ψ_l (following the lower path with the diffraction orders 0, p and $-p$):

$$\Psi_{u/l}(\mathbf{r}) = a_{u/l}\exp\left[i\left(\mathbf{k}\cdot\mathbf{r} + \varphi_{u/l}\right)\right] \quad (2)$$

with $a_u = \alpha_1(p)\alpha_2(-p)\alpha_3(0)$ and $a_l = \alpha_1(0)\alpha_2(p)\alpha_3(-p)$ while $\varphi_u = p\left[\mathbf{k}_{G1}\cdot(\mathbf{r}-\mathbf{r}_1) - \mathbf{k}_{G2}\cdot(\mathbf{r}-\mathbf{r}_2)\right]$ and $\varphi_l = p\left[\mathbf{k}_{G2}\cdot(\mathbf{r}-\mathbf{r}_2) - \mathbf{k}_{G3}\cdot(\mathbf{r}-\mathbf{r}_3)\right]$. These two waves interfere on the detector and the resulting total intensity is given by integrating over the detector surface:

$$\begin{aligned} I_1 &= \int d^2\mathbf{r}\,|\Psi_u + \Psi_l|^2 \\ &= \int d^2\mathbf{r}\left[a_u^2 + a_l^2 + 2a_u a_l\cos(\varphi_u - \varphi_l)\right]. \end{aligned} \quad (3)$$

To simplify the algebra, we have assumed that the amplitudes a_u and a_l are real. The phase $(\varphi_u - \varphi_l)$ is given by $\varphi_u - \varphi_l = p\left[\Delta\mathbf{k}_G\cdot\mathbf{r} + \Delta\varphi_G\right]$ where $\Delta\mathbf{k}_G$ is given by:

$$\Delta\mathbf{k}_G = \mathbf{k}_{G1} + \mathbf{k}_{G3} - 2\mathbf{k}_{G2} \quad (4)$$

and the phase $\Delta\varphi_G$ is a function of the grating positions only:

$$\begin{aligned} \Delta\varphi_G &= \left[2\mathbf{k}_{G2}\cdot\mathbf{r}_2 - \mathbf{k}_{G1}\cdot\mathbf{r}_1 - \mathbf{k}_{G3}\cdot\mathbf{r}_3\right] \\ &\approx k_G\left(2x_2 - x_1 - x_3\right). \end{aligned} \quad (5)$$

Fringes appear over the detector area if the condition $\Delta\mathbf{k}_G = 0$ is not fulfilled. In the experiments, this condition is verified by tuning the orientation of one grating in its plane and any small deviation induces a large visibility loss, as shown below (see Fig. 5). The x-positions of the three mirrors change the phase $\Delta\varphi_G$ of the atom interference fringes. This property provides a very convenient method to sweep the interference fringes: this phase is non-dispersive, i.e. independent of the velocity of the atomic wave, so that there is no associated visibility loss. If we assume that $\Delta\mathbf{k}_G = 0$, then $|\Psi_u + \Psi_l|$ is independent of $\mathbf{r}$ and the intensity I_1 of the exit beam B_1 is proportional to:

$$\begin{aligned} I_1 &= a_u^2 + a_l^2 + 2a_u a_l\cos(\varphi_u - \varphi_l) \\ &= I_{1,m}\left[1 + \mathcal{V}\cos(\varphi_u - \varphi_l)\right] \end{aligned} \quad (6)$$

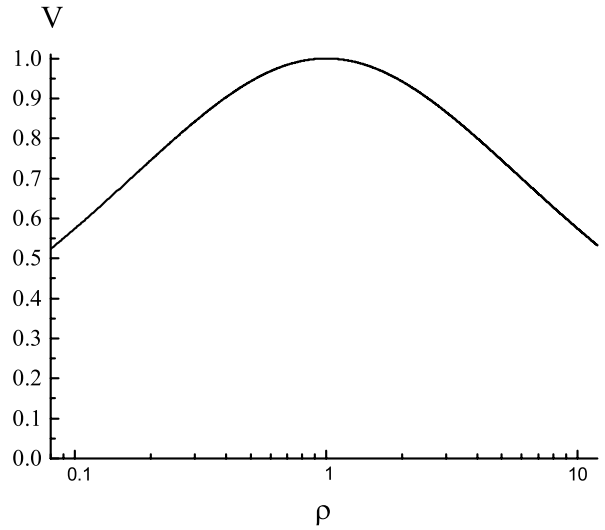

Fig. 2. Fringe visibility $\mathcal{V}$ for a two-beam interference as a function of the intensity ratio ρ. A logarithmic scale has been used for ρ so as to exhibit the symmetry when ρ is replaced by $1/\rho$.

where $\mathcal{V}$ is the fringe visibility given by:

$$\mathcal{V} = \frac{2a_u a_l}{a_u^2 + a_l^2} = \frac{2\sqrt{\rho}}{1+\rho} \tag{7}$$

where ρ is the ratio of the intensities carried by the two interfering beams, $\rho = a_u^2/a_l^2$. The visibility $\mathcal{V}$, which is a symmetric function of a_u and a_l, has the same value if ρ is replaced by its inverse. A small amplitude mismatch reduces the visibility but only very slightly, as shown in Figure 2.

2.2 Our main choices

Our goal was to build an atom interferometer in which the two atomic paths are sufficiently separated, so that one can apply a perturbation to only one path: such an arrangement is necessary to perform interferometric measurements of a perturbation. Previous experiments of this type include the measurement of the electric polarizability of sodium [20,21] and the measurement of the index of refraction of gases for sodium atomic waves [22,23], both experiments being done by Pritchard and co-workers. More recently, Toennies and coworkers have compared the electric polarizability of helium and helium dimer [24]. Moreover, we wanted to observe the dependence of the index of refraction with the velocity of the atomic wave and this dependence is detectable only if this velocity is comparable to or larger than the thermal velocity of the target gas. We have therefore chosen to use for the atomic wave a thermal beam rather than a slow beam: this second choice would have imposed to use also a cold atomic target, making the experiment very complex.

We had to choose the diffraction process, among several possibilities: diffraction by material gratings (which was first studied by Pritchard and co-workers [25] and briefly reviewed in Ref. [26]), elastic diffraction by a laser standing wave (first observed by Arimondo et al. [27], with well resolved diffraction peaks first recorded by Pritchard and co-workers [28]) or inelastic diffraction processes, which can be either a one-photon diffraction process (used in Ramsey-Bordé interferometers) [4], or a two-photon Raman diffraction process used in many cold or thermal atom interferometers (its first use being described in Ref. [5]). We have chosen to use elastic Bragg diffraction by laser standing waves, the main advantages being the high transmission of the interferometer associated with a high fringe visibility and the fact that we can use an ordinary single frequency laser. The first interferometers using this diffraction process and thermal atoms were built by Siu Au Lee and co-workers with metastable neon [12] and also by Zeilinger and coworkers using metastable argon (but not in the Bragg regime) [11]. Elastic diffraction is similar to diffraction by a material grating, in the sense that the internal atomic state is not modified. The grating period is equal to half the laser wavelength, which must be chosen very close to a resonance transition of the atom, so that diffraction can be observed with modest laser power densities. With sufficient laser power densities, diffraction orders higher than the first one can be easily observed [29–31].

The choice of laser diffraction limits the choice of the atom among those which have an intense resonance transition accessible to cw single frequency lasers. If one excepts the use of metastable states (with rare gases or hydrogen), this requirement favors considerably the alkali atoms. Then, the most important quantity is the Bragg angle $\theta_B = \lambda_{\rm dB}/\lambda_L$, which must be as large as possible in order to maximize the separation between the two atomic paths in the interferometer. Because the atomic de Broglie wavelength scales like m^{-1}, a light atom is favored and we have chosen the lithium atom. Its first resonance transition is at a 671 nm wavelength, corresponding to a grating period $a = 335$ nm. By seeding lithium in a supersonic beam of argon, the mean velocity u of the lithium atoms is close to 1060 m/s corresponding to a de Broglie wavelength $\lambda_{\rm dB} = 54$ pm and a Bragg angle $\theta_B = 80$ μrad.

2.3 Elastic diffraction of atoms by a laser standing wave

As pointed out by Siu Au Lee and coworkers [12], diffraction in the Bragg regime is ideal to build an interferometer: only two diffraction orders (0 and p) are produced for a well chosen incidence angle and, by varying the laser power density and/or the interaction time, the diffraction efficiency can be tuned to produce 50−50% beam-splitters and 100% mirrors. Therefore, the transmission of an ideal Mach-Zehnder interferometer using this diffraction process should be equal to 100% and, as a result of the symmetry of this interferometer, the fringe visibility, measured on the B_1 output beam, should also be equal to 100%.

We first recall that elastic diffraction by a laser standing wave results from the absorption of a photon going in one direction followed by the stimulated emission of a

photon going in the other direction: this scheme corresponds to first order diffraction and p steps are needed for the diffraction order p. After an absorption-emission cycle, the atom is back in its initial level, and it has received a momentum kick equal to two photon momenta.

The laser frequency ω_L and the resonance atomic frequency ω_0 differ by the detuning $\delta = \omega_L - \omega_0$, which must be considerably larger than the natural width γ of the resonance transition. Then, the main effect of the laser standing wave is to create a weak periodic potential proportional to the local density of energy in the laser beam, $V = V_0(z)\cos^2(k_L x)$ (where the x-axis is parallel to the laser beam wave vector). The periodic nature of the potential can be treated by introducing Bloch states as done in our previous paper [32], which quotes many previous works on laser diffraction.

To simplify the discussion, we assume that $V(z)$ extends over a distance w (we do not define precisely w which should not confused with the Gaussian beam radius w_0 discussed below), so that an atom with a velocity v interacts with the laser beam during an interaction time $t_{int} = w/v$. The natural energy unit of the problem is the atomic recoil energy $\hbar\omega_{rec} = (\hbar k_L)^2/(2m)$. Following [32,33], this quantity can be used to define a dimensionless potential $q = V_0/(4\hbar\omega_{rec})$ and a dimensionless interaction time $\tau = \omega_{rec} t_{int}$.

The incident atom is characterized by its momentum state in the x-direction, $|k_x\rangle$. When q is large ($q \gg 1$), the periodic potential couples the incident atomic wave $|k_x\rangle$ to many other states $|k_x + 2nk_L\rangle$, where n is an integer. The Bragg regime occurs when $k_x \approx \pm pk_L$ and if the potential q is not too strong and does not vary too rapidly with z. Then, one can neglect the coupling of the two states $|k_x = \pm pk_L\rangle$ with other states and treat the dynamics as a two-level problem. At the lowest nonvanishing order, the coupling between these two levels is proportional to q^p and the probability of diffraction of order p is then given by a Rabi oscillation:

$$P_p = \sin^2\left(q^p \tau / d_p\right) \tag{8}$$

where the coefficient d_p is equal to 1 for order $p = 1$, to 4 for order $p = 2$ and to 64 for order $p = 3$. The intensity which is not diffracted remains in the zeroth-order beam. Because of the dependence in q^p of the sine argument in equation (8), the q values for a 50−50% beam-splitter and a 100% reflective mirror are linked by $q_{BS} = q_M \times 2^{-1/p}$. Finally, this diffraction process induces some phase-shifts of the waves which will not discussed here but which may be very important [34].

If δ is too small, real excitation of the atom followed by a spontaneous emission of a photon occurs during the time spent by the atom in the laser field. When this occurs, the coherence of the atomic propagation is destroyed very efficiently. The probability P_{SE} of a spontaneous emission event is given by:

$$P_{SE} = q\tau\frac{\gamma}{\delta}. \tag{9}$$

As $q \propto \delta^{-1}$ and $P_{SE} \propto \delta^{-2}$, laser diffraction can be made almost perfectly coherent by choosing a sufficiently large detuning. For a given value of q, the use of a larger detuning requires also a larger laser power density, so that the available laser power gives a practical limit to the detuning.

3 Experimental set-up

Our experimental set-up is inspired by the sodium interferometer of Pritchard and co-workers [35] and by the metastable neon interferometer of Siu Au Lee and co-workers [12]. We are going to describe its main parts and to explain our procedures to align its components.

3.1 Vacuum system

The vacuum system is made of five differentially pumped chambers, (see Fig. 1):

- the first chamber contains the supersonic beam source and is pumped by a 8000 l/s unbaffled oil diffusion pump (Varian VHS400). The gas load due to the beam is a few mbar l/s and, under normal beam operation, the residual pressure is about 8×10^{-4} mbar. The beam exits this chamber through a 0.97 mm diameter skimmer provided by Beam Dynamics;
- the second chamber, which serves to differential pumping, to collimation and to optical pumping of the lithium beam, is pumped by a 2400 l/s oil diffusion pump (Varian VHS6) with a water cooled baffle. Under normal beam operation, the pressure is about 3×10^{-6} mbar. The beam exits this chamber through the source slit S_0;
- the third chamber, which serves to collimation only, is pumped by a 700 l/s oil diffusion pump from Edwards with an internal baffle. The residual pressure is below 5×10^{-7} mbar, practically independent of beam operation. The beam exits this chamber through the collimation slit S_1;
- the fourth chamber, which contains the interferometer, is pumped by two 1200 l/s oil diffusion pumps (Varian VHS1200) with water cooled baffles. The residual pressure is below 5×10^{-7} mbar. The detector slit S_D is also located in this chamber. The beam exits this chamber through a 3 mm diameter hole, located just before an UHV gate valve;
- the fifth chamber holds the surface ionization hot-wire detector. As the stray signal of such a detector is very sensitive to the residual gas, this chamber is built with UHV components and is pumped by a 300 l/s turbo molecular pump. The residual pressure in this chamber is a few 10^{-9} mbar, when the UHV gate valve is closed and about 10^{-8} mbar when it is opened.

All the water baffles are cooled by circulating a liquid near 3 °C. We use three double stage roughing pumps: two 65 m^3/h pumps, one for the beam source, one for the other four oil diffusion pumps and a 15 m^3/h pump for the turbo pump of the detector. To reduce vibrations induced in the set-up, these pumps are located in the next room.

3.2 The atom wave source and detector

Our lithium atomic beam, inspired by the design of Broyer, Dugourd and co-workers [36] is briefly described in [1,37,38] and more details will appear in another paper. Lithium is seeded in argon and our normal operating conditions are a source pressure of 330 mbar, a temperature equal to 973 K for the back part of the oven (fixing the lithium vapor pressure near 0.55 millibar), a temperature equal to 1073 K for its front part and a nozzle diameter equal to 200 μm. We have measured the beam mean velocity, $u = 1060$ m/s and the terminal parallel temperature of lithium $T_{\|} \approx 6.6$ K. This parallel temperature is roughly 1/3 of the calculated parallel temperature of the argon carrier gas, an effect which occurs when a light species is seeded in a heavier carrier gas [37,38].

To detect the output beams, we use a hot-wire detector which has been fully described in a previous study [39]. Its detection efficiency, which varies with the oxidation and the temperature of the rhenium wire, was measured to be close to 30%. With our normal operating conditions, the collimated beam gives a signal up to 8×10^4 counts/second, on a background signal close to 2×10^3 counts/second. This background signal presents a non-Poissonian statistics with a few bursts.

In Figure 1, it is clear that the location of the detector must be well chosen. We must put the detector far enough from the third laser standing wave, at a place where the two exit beams B_1 and B_2 are well separated: these beams carry complementary signals and the fringe visibility would be very small if the detector was put close to the third grating, where these two beams are strongly overlapping. The complementary character of the two signals is a consequence of the fact that laser diffraction is acting on the phase and not on the amplitude of the atomic wave (for more details, see Fig. 7 of Ref. [40]). However, we must not forget the existence of the stray beams represented in Figure 1. These beams carry some flux, because the diffraction amplitudes are not at their optimum values, and these stray beams cross the main exit beams B_1 and B_2 at a distance equal to the intergrating distance $L_{12} = L_{23} = 0.605$ m. Therefore, we have chosen to put the detector slit (which defines if an atom is detected or not) at a distance $L_{34} = 0.40$ m from the third laser standing wave, 0.2 m in front of the place where these stray beams are expected to create the largest signals. The hot wire itself is 0.35 m away in the fifth UHV vacuum chamber. In a first arrangement, the detection slit, which was placed very near the hot wire detector, was put out of order by excessive heating due to the hot wire radiation.

3.3 Laser standing waves

We use an home-made single frequency cw dye laser, following Biraben's design [41], pumped by a Spectra-Physics argon ion laser at 515 nm. The dye is LD 688 from Exciton dissolved in EPH. Using the Hänsch-Couillaud [42] frequency stabilization, we get a laser linewidth of the order of 1 MHz. The laser beam goes through a 60 dB optical isolator. After the isolator, the power available at 671 nm is close to 400 mW, for 5 W of Ar^+ pump power.

The laser frequency, which is measured by a home-made lambdameter, must be detuned from resonance, which has a complex structure due to the fine, hyperfine and isotopic splittings [43]. Most of our experiments are optimized for the ^{7}Li isotope (natural abundance 92.5%) and we define the frequency detuning by:

$$\delta/(2\pi) = \nu_L - \left(E(^2P_{3/2}) - E(^2S_{1/2}, F=1)\right)/h \quad (10)$$

where the energies are those of the ^{7}Li isotope levels. The hyperfine structure of the $^2P_{3/2}$ state is very small and can be neglected. Our usual choice of detuning is $\delta/(2\pi) = +3.0$ GHz and whenever a different value is used, it will be indicated. The natural width of the $^2S_{1/2}-^2P_{3/2}$ transition of lithium is $\gamma/2\pi = 5.9$ MHz [44].

The laser beam is magnified by a telescope made of two AR coated singlet lenses so that we can change the magnifying ratio by changing one lens. We characterize the beam transverse profile by scanning a photodiode through it, thanks to a motorized translation stage, and the recorded intensity as a function of the photodiode position is fitted to a Gaussian profile, thus extracting the Gaussian beam radius w_0. When operating with low power densities (practically only when using first order diffraction), the Gaussian beam is limited by an iris and the resulting beam profile is closer to a flat top profile.

The beam is then split by two beam splitters with a nominal transmission equal to 50% for an incidence of 45°. We thus get three beams, one with a power close to $P/2$ and two beams, each with a power close to $P/4$. The $P/2$ beam serves for the central laser standing wave, on mirror M_2, while the two $P/4$ beams serve for the other laser standing waves, on mirror M_1 and M_3. Using incidence angles different from 45°, we are able to modify the power repartition between these three beams: this is needed when using first order diffraction because the real transmission differs from 50% and also when using higher diffraction orders $p = 2$ and 3, because the needed power repartition is not the same. In order to choose the best laser power repartition, we have recently installed attenuators made of an half-wave plate followed by a polarizer on two of these three laser beams. This system was not available during most of the experiments described here.

The three laser beams are sent near normal incidence on the mirrors M_j. The properties of a standing wave are weakly sensitive to the exact value of the incidence angle on the mirror and very sensitive to the orientation of the direction perpendicular to the mirror surface. More precisely, if a plane wave is incident on a mirror with a small angle of incidence i, the reflected wave and the incident wave produce a wave which is progressive in a direction parallel to the mirror surface, with a wave vector $k_L \sin i$ and which is a standing wave in the direction normal to the mirror with a wave vector $k_L \cos i$. The progressive character of the wave parallel to the mirror surface induces a Doppler shift of its frequency equal to $k_L u \sin i$ which corrects the detuning: in our experiment, this Doppler shift of the order of 1.5 MHz per mrad is perfectly negligible.

The fact that the laser wave vector normal to the mirror surface is $k_L \cos i$ slightly modifies the momentum kick received by the atoms which becomes $2pk_L \cos i$ but, for small i values, this modification is negligibly small.

Following equation (6), the phase of the interference fringes depends on the x-positions of the three mirrors and this property makes the interferometer very sensitive to vibrations. In the interferometers developed by Pritchard [35] and by Siu Au Lee [12], these vibrations were controlled by servo-loops. We have chosen to minimize these vibrations by building a very rigid rail to support the three mirrors M_j. This rail and the role of vibrations will be discussed in an other paper. As in references [12,35], we use an optical three-grating Mach-Zehnder interferometer to control the vibrations of the x-positions of the three mirrors M_j and the measured noise on the quantity $(2x_2 - x_1 - x_3)$ is negligibly small, with a rms amplitude of the order of a few nanometers. The output signal of this interferometer is also used to calibrate the displacement of the motion of the mirror M_3, which serves to observe interference fringes.

3.4 Alignment procedures

We must align the atomic beam and the mirrors producing the laser standing waves. The numerous adjustments must be done with great care: to give an idea, most angles must finally be tuned within about 10 μrad from their optimum value.

The atomic beam alignment is difficult as the beam must go with minimum attenuation from the nozzle to the hot-wire of the detector 3.4 m away, through the skimmer, the source slit S_0, the collimation slit S_1, the detector slit S_D, the 3 mm diameter hole located before the detector chamber. For each element, we explain the available adjustments and how we proceed to make them:

- the oven can be adjusted in the three directions under operation;
- the skimmer and the 3 mm diameter hole are fixed to the center of their supporting flanges, while all the other elements can be adjusted in the **x**-direction, but not in the **y**-direction. This is possible because the three slits have a sufficient height, about 10 mm;
- the width of the slit S_0 is fixed and equal to 20 μm, while the widths of the collimation slit S_1 and of the detector slit S_D are controlled by piezo-drives from Piezosystem Jena in the $0-200$ μm range: the slit widths commonly used are $e_1 = 12$ μm for S_1 and $e_D = 50$ μm for S_D (if different values are used, they will be specified). The slit material has been chosen to be non magnetic, because the inhomogeneous field which would exist in the slit opening could induce a spreading of the atomic beam, by Stern and Gerlach effect;
- the slits S_0, S_1 and S_D are made vertical before operation. We have used either the diffraction pattern of a laser beam or the observation of the slit with a telescope, in comparison with a plumb line. We estimate that the slits are vertical within a few mrad: if the useful height of the slit S_i is h_i, a small error ϵ on its verticality induces no broadening of the full width at half maximum of the beam but a broadening of its wings of the order of ϵh_i. We can evaluate these useful heights simply by assuming straight lines trajectories for the atoms, from the skimmer to the 3 mm hole near the detector. The calculated useful height is 1.3 mm range for S_0, 1.8 mm for S_1 and 2.9 mm for S_D. The corresponding broadening of the beam wings, of the order of $1-3$ μm per mrad, is probably fully negligible for S_0 and S_D which are rather wide, and less negligible for S_1 which has usually the smallest width;
- the x-position of these three slits and of the hot-wire can be modified under vacuum: in each case, we use a translation stage operated by a linear drive vacuum feedthrough, with a sensitivity of the order of 10 μm. In addition, the x-position of the detector slit S_D can be swept under computer control by a piezo-translation from Piezosystem Jena over 400 μm.

For the laser standing waves, each mirror M_j is attached to a double stage kinematic mount built in our laboratory. The first stage, with screws, can be operated only when the experiment is at atmospheric pressure while the second stage actuated by low-voltage piezo-translators, has a tuning range close to 600 μrad. A first alignment, within ± 100 μrad, must be made with the experiment at atmospheric pressure and the final tuning is made with the second stage. To make the first alignment, we use the following signals:

- we first adjust the rotation θ_z around the horizontal axis **z** with an autocollimator. For each mirror M_j, we set the autocollimator by observing the horizontal surface of diffusion pump oil through a pentaprism and we set the mirror perpendicular to the autocollimator axis;
- we then adjust the rotation θ_y around the vertical axis **y**, with a laser beam which replaces the atomic beam, going from the skimmer to the 3 mm hole near the detector. Then, using a pentaprism, we send this beam successively on each mirror M_j and we set the mirror so as to maximize the reflected laser power measured behind the skimmer.

With the experiment under vacuum, we make the final adjustment of θ_y for each mirror M_j: we tilt the mirror to observe Bragg diffraction of the chosen order p (see Fig. 3) with the corresponding laser standing wave. We have no signal which can be used to finely tune the θ_z angles separately, but we must tune one of these three angles to cancel $\Delta\mathbf{k}_G$ defined by equation (4) and the fringe visibility is very sensitive to an exact cancellation, as shown below in Figure 5. We use mirror M_2 as its effect is twice as large as the effect of M_1 or M_3.

Finally, an optical grating is linked to each mirror M_j to form the optical three-grating Mach-Zehnder interferometer briefly discussed above. It is necessary to align this interferometer before the final adjustments of the mirrors M_j.

Table 1. This table collects information concerning our best signals obtained with the diffraction order p. We give the date of the experiment, the mean intensity I_0, the visibility $\mathcal{V}$ and several experimental parameters: the Gaussian beam radius w_0, the laser detuning $\delta/(2\pi)$, the total laser power P used in the laser standing waves, the collimation slit width e_1 and the detection slit width e_D. We have also calculated the figure of merit $I_0\mathcal{V}^2$, related to the phase sensitivity if Poissonian statistics is assumed; (a) when using $p = 1$, the intensity profile has a flat top and w_0 is the radius of the laser beam, (b) experiment done with a cancellation of the effect of the magnetic field gradient, (c) not measured during the experiment.

p	Date	I_0 (c/s)	$\mathcal{V}$ %	$I_0\mathcal{V}^2$	w_0 (mm)	$\delta/(2\pi)$ (GHz)	P(mW)	$e_1(\mu$m)	$e_D(\mu$m)
1	March 2004	12900	80.5 ± 1	8360	5.0 (a)	2.8	150	12	40
	July 2004 (b)	23710	84.5 ± 1	16930	5.0 (a)	2.8	150	12	40
2	April 2004	14430	49.0 ± 1	3465	2.9	1.5	300	12	50
	Sept. 2004	20180	51.0 ± 1	5250	1.8	3.1	460	14	50
	Sept. 2004 (b)	8150	54.0 ± 1	2735	1.8	3.1	(c)	14	60
3	April 2004	4870	26.0 ± 1	304	2.9	1.1	300	12	40

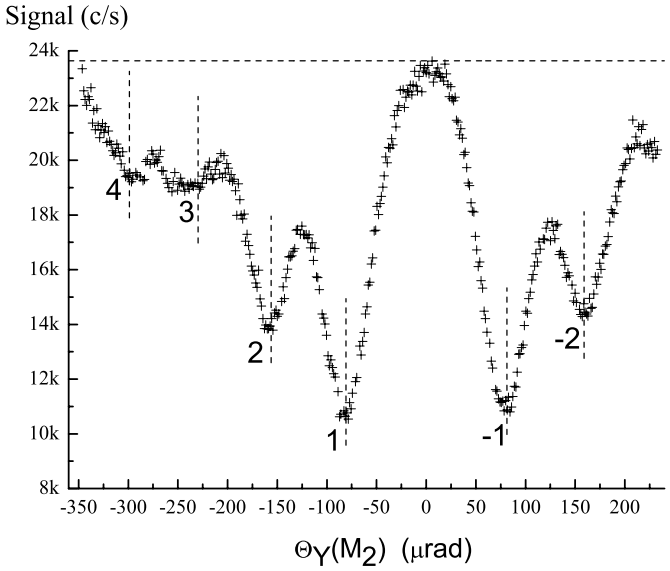

Fig. 3. Intensity of the direct beam measured as a function of the angle θ_y of mirror M2. When the Bragg condition is fulfilled for a diffraction order p, the transmitted intensity goes through a minimum labelled by the order p. This experiment was made with an almost Gaussian laser beam with a measured waist radius $w_0 = 3.1$ mm, a power $P = 240$ milliwatts and a detuning $\delta/(2\pi) = 1.2$ GHz. The collimation slit width was $e_1 = 10$ μm and the detection slit was $e_D = 70$ μm.

4 Atom interference effects

4.1 Diffraction experiments

With only one laser standing wave, we can observe diffraction. Two main types of diffraction experiments have been done:

- by setting the orientation of the mirror in order to be in the Bragg geometry, we produce a diffracted beam. Then, by scanning the position of the detector slit, we can record the profile of the direct and diffracted beam. A typical result was shown in our previous paper [1]. We have verified that the diffraction behaves as expected in the Bragg regime, with, in particular, the absence of a beam of order $p = -1$ when the geometry favors the diffraction of order $p = 1$;
- by rotating the mirror around the y-axis, we successively fulfill the Bragg condition for the various diffraction orders p. We have recorded the direct beam intensity as a function of the angle θ_y and diffraction then appears as an intensity loss. Figure 3 presents such a recording. We observe intensity losses corresponding to Bragg condition for the orders $p = -2$ up to $p = 4$. The interest of such a recording is that it gives immediately an idea of the diffraction efficiency. We never reach a 100% diffraction probability, because of the presence of ^{6}Li and of the finite widths of the velocity and angular distributions of the incident atomic beam.

With our usual detuning $\delta/(2\pi) = 3.0$ GHz and with the typical power density used for first order diffraction, the diffraction probability for the ^{6}Li atoms is very small and we may forget their presence. We have also made some experiments with a detuning chosen to diffract selectively these atoms.

4.2 High visibility atom interference fringes

We have operated our interferometer using successively three different diffraction orders $p = 1$, 2 and 3. By sweeping the x-position of mirror M_3, we have observed interference signals with a very high visibility which are plotted in Figure 4. In all cases, the signal is expressed as a number of atoms detected per second with an usual counting time equal to 0.1 s. The observed signal can be written as:

$$I_1 = I_B + I_0\,[1 + \mathcal{V}\cos\phi]\,. \tag{11}$$

The background signal I_B of the detector is recorded just after or before recording the signals, by flagging the atomic beam in the second chamber and we deduce from this measurement the mean I_B value. Then, we can make a fit of the signal to estimate the mean intensity I_0 and the visibility $\mathcal{V}$. The phase ϕ is a locally linear function of time, but the fit must take into account the nonlinearity of the piezo drive. Table 1 gives for the three orders $p = 1$, 2 and 3 the parameters used (laser detuning, beam waist w_0 and

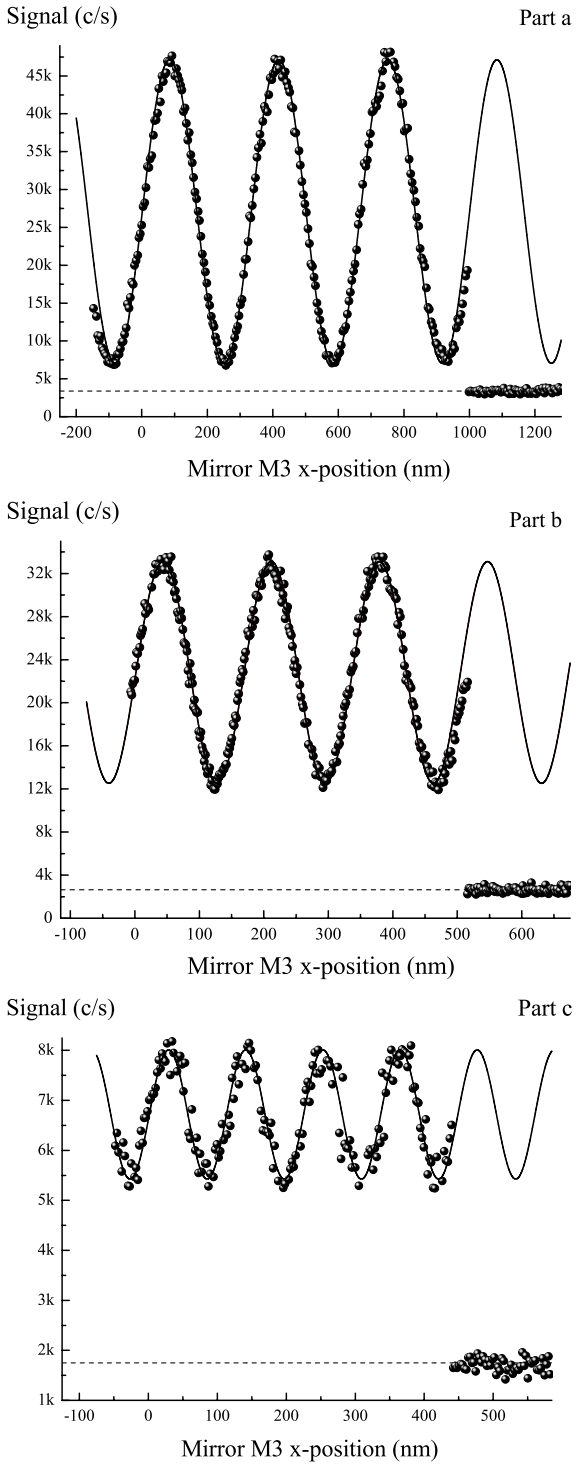

Fig. 4. Interference signals recorded with the diffraction orders $p = 1$ (part a, 84.5% visibility, collimation slit width $e_1 = 12\ \mu$m, detection slit width $e_D = 40\ \mu$m), $p = 2$ (part b, 51% visibility, $e_1 = 14\ \mu$m, $e_D = 50\ \mu$m) and $p = 3$ (part c, 26% visibility, $e_1 = 12\ \mu$m, $e_D = 40\ \mu$m). In these three cases, the B_1 output signal is measured as a function of the x-position of mirror M_3, calibrated thanks to the optical interferometer linked to the three mirrors. The counting time is equal to 0.1 s and one can see that the displacement Δx necessary to sweep one fringe is equal to $\lambda_L/(2p)$. The background signal recorded just after the recording of the signal is also plotted.

beam powers) and the mean intensity I_0 and the visibility $\mathcal{V}$ deduced from the fits.

We have measured the interferometer transmission by making the ratio of the intensity at the peak of constructive interference and of the intensity of the direct atomic beam, in the absence of the three laser standing waves. With first order diffraction, the measured transmission can reach quite large values, up to 85%. Theory predicts a 100% value and the difference is due mainly to imperfections of the diffraction process and to the presence of ^{6}Li in the beam with its natural abundance equal to 7.5%.

The dependence of the fringe visibility with the diffraction order has been studied only once before, by Siu Au Lee and coworkers [12]: in this experiment like in the present case, the visibility decreased rapidly with increasing order: $\mathcal{V} = 62\%$ for $p = 1$, $\mathcal{V} = 22\%$ for $p = 2$ and $\mathcal{V} = 7\%$ for $p = 3$. The most natural explanation of this rapid decrease is the existence of a phase noise with an amplitude proportional to the diffraction order p: this is the case if the phase noise comes from the grating vibrations. However, two other effects may also contribute to the rapid decrease of the fringe visibility when the order p increases:

- the incoherent processes involving a real photon absorption followed by spontaneous emission are not negligible with the power densities used for orders $p = 2$ or 3;
- the diffraction phase-shifts [34] behave like $q^2\tau$ and may be rather large during the diffractions of orders $p = 2$ or 3. A large phase shift does not induce a loss of fringe visibility if it is the same for all the atoms. The dependence of the phase shift with time (due to the intensity fluctuations of the laser), with space (due to the intensity profile of the laser beams) and with the atom velocity may result in a large reduction of the fringe visibility.

We think that decoherence by collision with the residual gas is negligible in our case. This decoherence effect, which has been studied in a Talbot-Lau interferometer with fullerenes [45–47], could be observed in our case if a lithium atom can be detected with a large probability even after a collision with an atom of the residual gas. Obviously, this is not the case. The residual gas creates an index of refraction proportional to its density and the transmitted waves are attenuated and phase shifted [22,23]. The fluctuations of these phase shifts could induce a phase noise and a reduction of the fringe visibility, but this effect is negligible in our experiment. Moreover, this decoherence effect has no strong dependence with the diffraction order p.

By moving the detector slit, we have successively recorded the interference signals on the two outputs beams, B_1 and B_2, and we have verified that a destructive interference at B_1 corresponds to a constructive interference at B_2. The observed visibility at B_2 is slightly less good than at B_1: the simplest explanation, which would be that the two interfering beams have not equal amplitudes, is not convincing (see Eq. (7) and Fig. 2). We think

that the visibility difference is most probably due to the stray beams represented in Figure 1.

We have also been able to observe signals due to the ^{6}Li isotope present in the lithium beam with its natural abundance (7.5%). This was done by changing the laser frequency so that the diffraction was isotopically selective in favor of ^{6}Li: for this experiment, we used a laser frequency with a detuning of $\delta/(2\pi) \approx -24$ GHz, so that the laser is at 4 GHz on the red side of the $^2S_{1/2}-^2P_{1/2}$ transition of the ^{6}Li isotope and at 14 GHz on the red side of the nearest transition of the ^{7}Li isotope, which is also the $^2S_{1/2}-^2P_{1/2}$ transition. We thus observe a mean intensity $I_0 = 4240$ s^{-1} and a visibility $\mathcal{V} = 55\%$. Considering the 7.5% natural abundance of ^{6}Li, the observed mean intensity is too high to be purely ^{6}Li; we think that a noticeable contribution comes from the ^{7}Li content of various stray beams (with the detuning used, the probability of diffraction of ^{7}Li atoms by one of the three laser standing waves is small but not fully negligible). As these stray beams carry no interference effect, their contribution to the signal could explain a too large value of the mean intensity and, at the same time, a visibility which is smaller than what we observe with when we work with ^{7}Li.

5 Optimization of the fringe visibility

We have explored how the defects modify the fringe visibility in a systematic way. These effects can be analyzed theoretically [40,48] and we will compare the results of this analysis with our experimental results.

5.1 Sensitivity of the visibility to the orientations of the standing wave mirrors

We have not made any systematic study of the effect of the rotations around the **y**-axis: these rotations modify the angle of incidence of the atomic wave on the laser standing wave. When this angle differs sufficiently from the Bragg angle, the diffraction amplitude is reduced. The output signal and the fringe visibility should also be reduced, but, following equation (7), the associated visibility reduction is expected to be very slow. On the contrary, the rotation around the **z**-axis has a very large effect, as explained by the simple plane wave theory recalled in Section 2.1. The two waves, which interfere on the detector, present a wave vector difference equal to:

$$\Delta\mathbf{k} = p\,(2\mathbf{k}_{G2} - \mathbf{k}_{G1} - \mathbf{k}_{G3})\,.$$

The signal comes from the integration over the detector surface of the local intensity. If we assume that a flat intensity profile over a region $-h_D/2 < y < h_D/2$ and zero intensity elsewhere, we calculate a visibility given by:

$$\mathcal{V} = \mathcal{V}_0\,|\,\mathrm{sinc}\,(\Delta k_y h_D)| \qquad (12)$$

where $\mathcal{V}_0$ stands for the visibility achieved when $\Delta\mathbf{k} = 0$, Δk_y is the y component of $\Delta\mathbf{k}$ and sinc(x) is a short-hand notation for $\sin(x)/x$.

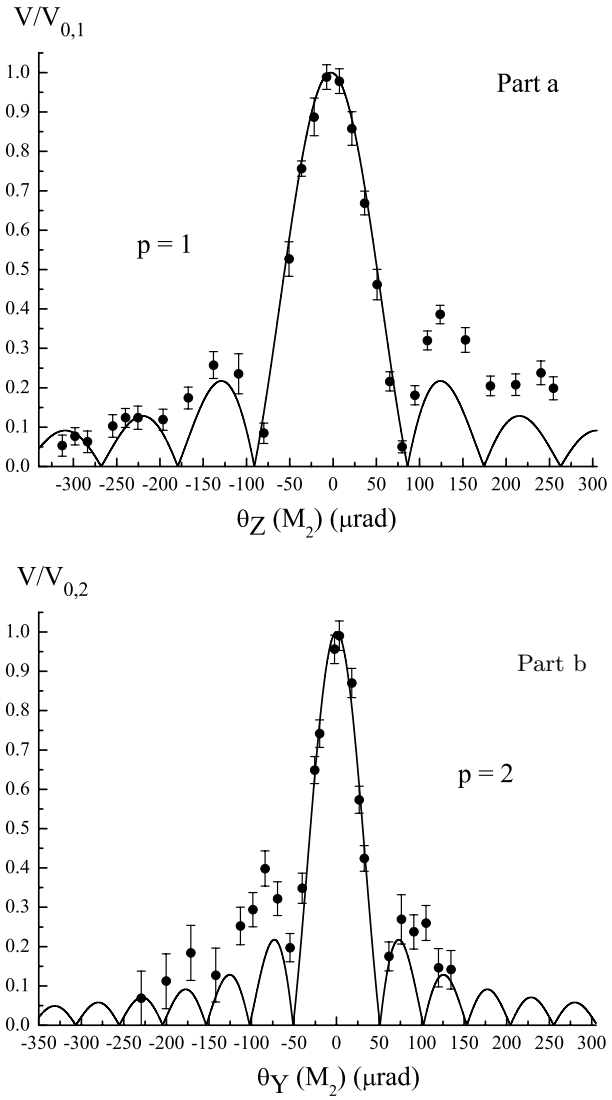

Fig. 5. Fringe visibility measured as a function of the angle θ_z measuring rotation around the **z**-axis of mirror M_2. The experiment has been done with the diffraction orders $p = 1$ (part a) and $p = 2$ (part b). The points are experimental and the curves are the best fits using equation (12). The agreement is excellent in the central region, where the visibility decreases twice as fast as when using $p = 2$ than when using $p = 1$, in agreement with equation (12).

We have tilted mirror M_2 around the **z**-axis, by applying a voltage on the corresponding piezo-drive and we have recorded fringes and measured their visibility. We have converted the voltage applied on the piezo-drive into a rotation angle, using an external calibration and neglecting the piezo hysteresis. The measured visibility has been plotted as a function of the angle $\theta_z(M_2)$ in Figure 5. The visibility decreases rapidly, as expected, but it does not vanish where predicted by equation (12). We think that this is a kind of apodization effect: the predicted cancellations disappear if a smooth weight function of y replaces the 0 or 1 intensity function used to establish equation (12).

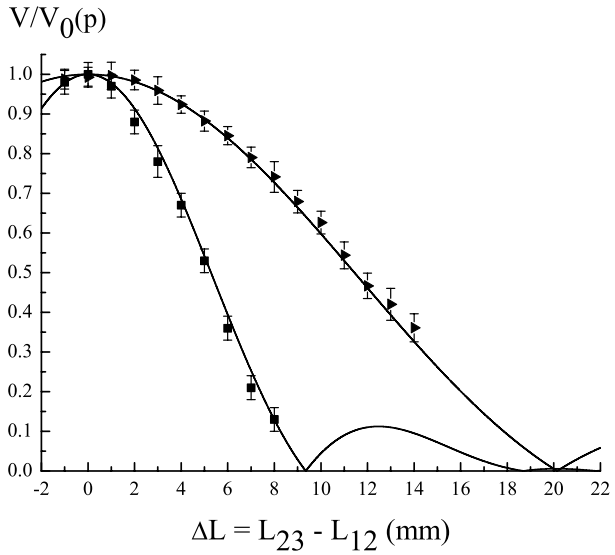

Fig. 6. Fringe visibility as a function of the mismatch between the distances between consecutive gratings $\Delta L = L_{23} - L_{12} = z - z_c$ for first (triangles) and second (squares) diffraction orders. The points are experimental and the curve is the best fit using our approximate formula (Eq. (13)), for a collimation slit width $e_1 = 14$ μm. The fitted parameter are the maximum visibility $\mathcal{V}_0(p)$ for each order p and the position z_c corresponding to a vanishing distance mismatch.

Pritchard and co-workers have made a study very similar to the present one in [35].

5.2 Fringe visibility as a function of the mismatch between the distances between consecutive gratings

If the distances between consecutive gratings L_{12} and L_{23} are different, the symmetry of the Mach-Zehnder interferometer is broken and the visibility is reduced. This effect was studied by numerical simulation by Turchette and coworkers [48]. We have shown [40] that, if the diffraction due to the slit S_1 is negligible, the visibility is given by:

$$\mathcal{V} = \mathcal{V}_0 \left| \text{sinc}\left(\frac{pk_G e_0 \Delta L}{2L_{04}}\right) \text{sinc}\left(\frac{pk_G e_D \Delta L}{2L_{04}}\right)\right| \quad (13)$$

where $\Delta L = L_{23} - L_{12}$ (this formula was written in [40] for the diffraction order $p = 1$ only).

To study this effect, we have moved the last mirror encountered by the laser beam on its way to the mirror M_1 where it reflects and forms the first laser standing wave. This motion was done with a translation stage, so that the laser beam direction is conserved. For various positions z of this translation stage, we have recorded atom interference signals and measured their fringe visibility $\mathcal{V}$. The measurements have been fitted by equation (13), in which we have replaced $\Delta L = z - z_c$, where z_c corresponds to the position which cancels the mismatch ΔL. The data points and their fit are plotted in Figure 6 and the agreement is very good. We cannot explore a larger range of z values because of the limited window diameter. By a direct measurement on our machine, we have verified that the value of $z_c = 3.5$ mm deduced from the fit corresponds well, with an uncertainty of ± 0.5 mm, to the equality of the two distances L_{12} and L_{23}.

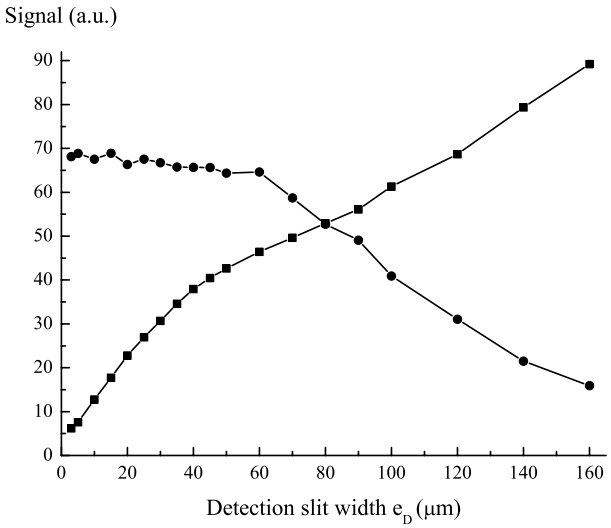

Fig. 7. Fringe visibility $\mathcal{V}$ in % (dots), and mean signal intensity I_0 in 10^3 counts/s (squares) as a function of the detector slit width e_D in μm while the collimation slit width is $e_1 = 12$ μm. The lines are simply drawn to guide the eye.

5.3 Signal and fringe visibility as a function of slit widths

The widths of the collimation and detector slit can be adjusted by piezo actuators and they open symmetrically. We have varied these two slit widths and we have recorded the interference signals on which we have measured the fringe visibility $\mathcal{V}$ and the mean intensity I_0. These two quantities are plotted as a function of the detector slit width e_D in Figure 7 and as a function of the collimation slit width e_1 in Figure 8. This study is very useful to optimize the phase sensitivity of the interferometer.

If we consider first Figure 7 representing the effects of the detector slit width e_D, the signal intensity I_0 increases linearly with e_D up to $e_D \approx 40$ μm while the visibility $\mathcal{V}$ is roughly constant as long as $e_D < 60$ μm: this first regime is what is expected when the detector slit collects only the signal corresponding to beam B_1. Then for larger e_D values, the intensity I_0 increases more slowly and the visibility $\mathcal{V}$ decreases rapidly. Now, the detector slit is sufficiently opened to collect all the B_1 beam and a part of the B_2 beam. If the interferometer was perfectly symmetrical, the B_2 beam would carry the same flux as B_1 beam with a complementary interference signal. The fact that the intensity increases with a slope reduced roughly by a factor 2 is in agreement with the fact that the slit opens symmetrically and only one side of the slit is useful to transmit the B_2 beam and the rapid decrease of the visibility is in good agreement with the fact that the two beams B_i carry complementary interference signals.

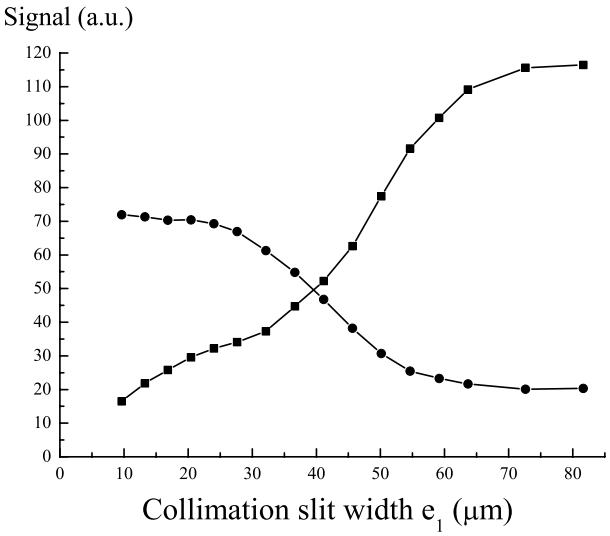

Fig. 8. Fringe visibility $\mathcal{V}$ in % (dots) and mean signal intensity I_0 in 10^3 counts/s (squares) as a function of the collimation slit width e_1 in μm while the detection slit width is $e_D = 43$ μm. The lines are simply drawn to guide the eye.

When the collimation slit width e_1 is varied, the effects are slightly more complex. In particular, one should not forget that Bragg diffraction has a strong angular selectivity: this selectivity makes that when the slit is widely opened, it admits in the interferometer atoms which have not the Bragg incidence and therefore these atoms have a low diffraction probability. These atoms will contribute to make the direct stray beam (the beam which is diffracted three times in the zeroth order) more intense. As long as the collimation slit width e_1 is below 25 μm, the intensity I_0 increases with the slit width while the contrast is mostly constant. When $35 < e_1 < 70$ μm, the intensity increases more rapidly, as a consequence of the broadening of the wings of the direct beam. As the direct beam carries no interference signal, the visibility decreases while the product $I_0\mathcal{V}$ remains roughly constant. Finally, when $e_1 > 70$ μm, the intensity saturates because the direct stray beam fully covers the detection slit and the visibility remains constant.

5.4 Fringe visibility as a function of an applied magnetic field gradient

An atomic Mach-Zehnder interferometer operating with paramagnetic atoms like lithium remains insensitive to a weak homogeneous magnetic field but the output signal is very sensitive to a magnetic field gradient, as explained below. This effect was studied by Pritchard and co-workers [35,51] and also by Giltner in his thesis [52].

In our experiment, the Earth magnetic field is not compensated. Moreover, the vacuum pipes are supported by a very heavy structure made of steel rails, but we have made efforts to use very few magnetic parts inside the interferometer vacuum chamber, the only exception being small steel springs in the kinematic mounts of the three mirrors. The field along the atomic paths has been measured, it is very roughly homogeneous, reminiscent of the Earth field (of the order of 4×10^{-5} T) and an important point is that it never vanishes.

We assume that the field is weak, below 10^{-3} T, so that the hyperfine structure remains coupled: the eigenstates are the $|F, M_F\rangle$ sublevels and it is a good approximation to consider only first order Zeeman effect. As the field never vanishes, the adiabatic theorem can be applied and the projection M_F of the angular momentum remains constant on a quantization axis which follows the local direction of the field. The magnetic phases $\phi(F, M_F)$ are given by:

$$\phi(M_F) = \frac{g_F \mu_B M_F}{\hbar v} \int B(s) ds \tag{14}$$

where g_F is the hyperfine Landé factor, B is the modulus of the magnetic field and the integral is carried along the atomic path. Neglecting the nuclear spin contribution to the atomic magnetic moment, for lithium ^{7}Li, the nuclear spin is $I = 3/2$ and the hyperfine levels with $F = 1$ and 2 have opposite Landé factors equal to $g_F = -1/2$ for the $F = 1$ and $g_F = +1/2$ for the $F = 2$.

The magnetic phases are quite large, $\phi(M_F)/M_F = 2 \times 10^3$ rad for a field $B = 4 \times 10^{-5}$ T. Fortunately, these phases play no role in the absence of non-adiabatic transitions from one sublevel to another one. The interferometer signal is only sensitive to the phase difference for each sublevel between the two atomic paths. In the presence of a gradient of the magnetic field modulus B in the x-direction, the interference pattern corresponding to the M_F level suffers a phase shift $\Delta\phi(F, M_F) = \varphi M_F$ with φ given by:

$$\varphi = \frac{g_F \mu_B}{\hbar v} \int \frac{dB(s)}{dx} \Delta x(s) ds \tag{15}$$

where $\Delta x(s)$ is the distance between the two atomic paths. Let us consider a magnetic dipole μ parallel to the **x**-axis, located at a distance d from the atomic paths. We can get a closed form expression of φ if we neglect the homogeneous background field and if we assume that $\Delta x(s)$ is almost constant over the region where the gradient of B is large, we get:

$$\int \frac{dB(s)}{dx} ds = \frac{\mu_0 \mu}{2\pi d^3} \int_{-\pi/2}^{\pi/2} \left[3\cos^2\theta + 1\right]^{1/2} \cos\theta d\theta \tag{16}$$

where the integral over θ is equal to 3.42. One must not forget that the approximations made are not very good. With ^{7}Li hyperfine level structure, in the absence of optical pumping, i.e. assuming the same population for the 8 sublevels, the interference visibility varies with φ in the following way:

$$\mathcal{V} = \mathcal{V}_0 \frac{2 + 4\cos\varphi + 2\cos 2\varphi}{8}. \tag{17}$$

With our approximations, φ is a linear function of the dipole moment or of the current if we use a coil. Moreover φ is proportional to v^{-2}, where v is the atom velocity: a v^{-1} factor is obvious in equation (15) and the other

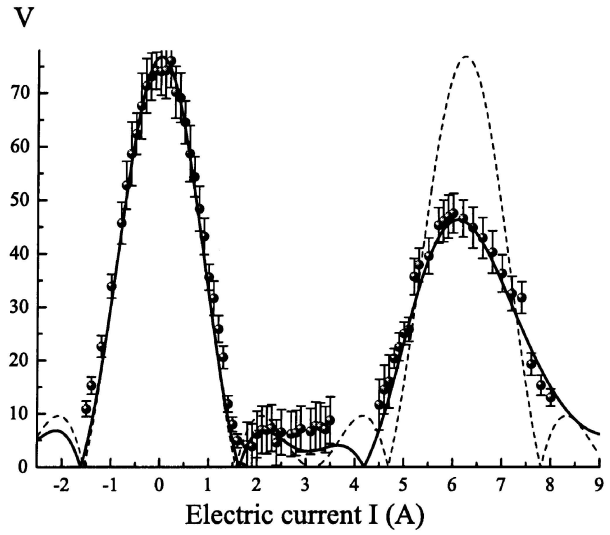

Fig. 9. Fringe visibility $\mathcal{V}$ as a function of the electric current I in the coil which creates a magnetic gradient over the atomic paths. The points are experimental while the full curve is the best fit using equations (17) and (19) with $\alpha/u = 0.111$, a value rather close but lower than the one measured on our incident lithium beam $\alpha/u = 0.133$, showing the selectivity of the Bragg diffraction process. The dashed curve is the curve predicted if the velocity was perfectly defined and equal to u (i.e. if $\alpha = 0$).

factor is hidden in the quantity $\Delta x(s)$ proportional to the diffraction angle.

The velocity distribution of the lithium atoms induces a dispersion on φ which further induces a fringe visibility reduction. Assuming a Gaussian velocity distribution profile $P(v)dv \propto \exp[-(v-u)^2/\alpha^2]$, we deduce a phase distribution:

$$P(\varphi)d\varphi \propto \exp\left[-\left(\varphi-\varphi_m\right)^2/\beta^2\right] \qquad (18)$$

with the phase φ_m corresponding to the velocity u and $\beta = 2\varphi_m\alpha/u$. This approximate formula is valid in the limit $\alpha \ll u$. After averaging over φ, the visibility $\mathcal{V}$ is then still given by equation (17), where $\cos(k\varphi)$ (k is an integer) is replaced by its average $\langle\cos(k\varphi)\rangle$ over the distribution $P(\varphi)$ simply given by:

$$\langle\cos(k\varphi)\rangle = \cos(k\varphi_m)\exp\left[-k^2\beta^2/4\right]. \qquad (19)$$

We have done a first experiment with a coil outside the vacuum tank. The coil, with 350 turns and a mean turn area close to 50 cm^2, is located at about 20 cm from the atomic paths. We have recorded interference fringes for different currents I, varying from 0 to 8 A by 0.1 A steps. We have measured the fringe visibility $\mathcal{V}$, which is plotted as a function of the current I in Figure 9. Because of the dispersion on φ due to the velocity distribution of the lithium atoms, the visibility observed at the peak of the revival is not as large as when $\varphi = 0$. As a consequence, the variation of the visibility with the applied field gradient contains an information on the velocity dispersion of the atoms contributing to the atomic interference signal. As Bragg diffraction is velocity selective, this velocity distribution may differ from the velocity distribution of the lithium beam measured at the entrance of the interferometer [37,38]. The present arrangement with a large coil rather far from the atomic path is not very favorable for a precise analysis, because the applied field is perturbed by the magnetic parts of the set-up, but with an improved arrangement, we hope to measure accurately the velocity distribution of the atoms contributing to the interference signal.

Recently, we have used a small coil under vacuum (3.5 turns of wire on a 3 cm diameter ring, with the coil center at a distance $d = 7.5$ mm from the atomic paths). In a first time, we have studied with care the region of near zero field gradient and we have observed an improved fringe visibility for a small current in the coil, thus proving that a small but non negligible magnetic field gradient is present in our apparatus. In such an experiment, we do not cancel everywhere the magnetic field gradient but we simply cancel the integral appearing in equation (15). In this experiment, the best observed visibility is $\mathcal{V} = 84.5 \pm 1.0\%$ for the diffraction order $p = 1$ and $\mathcal{V} = 54.0 \pm 1.0\%$ for the diffraction order $p = 2$ and these results are presented in Figure 4.

The effect of an electric field gradient exists also and it has been used recently [21] for the compensation of phase dispersion in an atom interferometer. The Stark effect is quadratic in electric field and, in a $^2S_{1/2}$ state, it is, with an excellent approximation, independent of the F, M_F sublevel as a consequence of the Wigner-Eckart theorem. The induced phase is the same for all the F, M_F levels and this phase will play a role only if it is large, because of its dispersion with the atom velocity. A large phase will exist only if the electric field and its gradient are both large enough. The stray electric field normally encountered inside vacuum chambers are usually weak, below 1 V/cm, and we do not expect a large gradient, especially close to the metallic rail supporting the mirrors. The resulting loss of coherence due to the stray electric field should be fully negligible.

6 Conclusion

In this paper, we have described our Mach-Zehnder atom interferometer operating with a thermal lithium beam and we have shown some examples of the observed signals. We have briefly recalled the main theoretical points, as they are very important to choose the best parameters. We have then given a description of this interferometer and its operation: vacuum system, laser system and laser standing waves, alignment procedures, the other parts being the subjects of separate publications.

In our interferometer like in the metastable neon interferometer of Siu Au Lee and coworkers [12], the mirrors and beam-splitters for the atomic waves are based on elastic diffraction by laser standing waves, in the Bragg regime. This choice provides an almost ideal interferometer and, in agreement with the theory of such interferometers, we have measured a high transmission and an

excellent visibility, $\mathcal{V} = 84.5 \pm 1.0\%$, when using first order diffraction: this is the best visibility ever achieved with a thermal atom interferometer with spatially separated atomic paths. This observation proves that the atom propagation is almost perfectly coherent in the interferometer: the two atomic paths are separated by 100 μm, in the vicinity of the second laser standing wave and this distance is close to 2×10^6 de Broglie wavelengths!

We have also operated our interferometer with the diffraction orders $p = 2$ and 3. The fringe visibility diminishes rapidly with the diffraction order p and we are presently investigating the origins of this rapid diminution. We have also tested the effect of the main misalignments on the fringe visibility, with results in excellent agreement with theory. We have studied the signal intensity and the fringe visibility as a function of the width of the collimation and detector slits.

This study will serve to optimize the operating conditions and to reach the best phase sensitivity, which is a very important point for the accurate measurement of perturbations. We have achieved a phase sensitivity close to 25 mrad/$\sqrt{\text{Hz}}$ which is better than the 34 mrad/$\sqrt{\text{Hz}}$ obtained in our previous study [1] (an error was made in this paper and we gave a value which was too small by a factor 2). With minor improvements, we hope to measure phase shifts with an accuracy close to 1 mrad in a few minutes of experiment.

Finally, following previous experiments, we have applied a magnetic field gradient: when the gradient increases, the fringe visibility first decreases and vanishes, before presenting a revival for a larger gradient. The intensity of the visibility revival is a sensitive tool to measure the velocity spread of the atoms contributing to the interferometer signal.

We are going to proceed now to interferometric measurements: our first goals are the measurements of the electric polarizability of lithium atom and of the index of refraction of permanent gases for lithium waves. The possibility of using several diffractions orders may reveal very interesting in this case, as the path separation is proportional to the diffraction order.

We are very much indebted toward R. Delhuille, who was the first to operate successfully this atom interferometer in 2001. We also thank C. Champenois, L. Jozefowski for their important contributions to the early phase of this work, and L. Lazar, for her participation to the magnetic rephasing experiment. Special thanks to F. Biraben and F. Nez for their loan of material, to D. Pritchard and Siu Au Lee for various information concerning their experiments. We thank CNRS SPM, Région Midi-Pyrénées, université Paul Sabatier and IRSAMC for financial support.

References

1. R. Delhuille, C. Champenois, M. Büchner, L. Jozefowski, C. Rizzo, G. Trénec, J. Vigué, Appl. Phys. B **74**, 489 (2002)
2. O. Carnal, J. Mlynek, Phys. Rev. Lett. **66**, 2689 (1991)
3. D.W. Keith, C.R. Ekstrom, Q.A. Turchette, D.E. Pritchard, Phys. Rev. Lett. **66**, 2693 (1991)
4. F. Riehle, Th. Kisters, A. Witte, J. Helmcke, Ch.J. Bordé, Phys. Rev. Lett. **67**, 177 (1991)
5. M. Kasevich, S. Chu, Phys. Rev. Lett. **67**, 181 (1991)
6. *Atom interferometry*, edited by P.R. Berman (Academic Press, 1997)
7. U. Sterr, K. Sengstock, J.H. Müller, D. Bettermann, W. Ertmer, Appl. Phys. B **54**, 341 (1992)
8. A. Morinaga, T. Tako, N. Ito, Phys. Rev. A **48**, 1364 (1993)
9. Ch.J. Bordé, N. Courtier, F. du Burck, A.N. Goncharov, M. Gorlicki, Phys. Lett. A **188**, 187 (1994)
10. M.S. Chapman, C.R. Ekstrom, T.R. Hammond, R.A. Bernstein, J. Schmiedmayer, S. Wehinhger, D.E. Pritchard, Phys. Rev. Lett. **74**, 4783 (1995)
11. E.M. Rasel, M.K. Oberthaler, H. Batelaan, J. Schmiedmayer, A. Zeilinger, Phys. Rev. Lett. **75**, 2633 (1995)
12. D.M. Giltner, R.W. McGowan, Siu Au Lee, Phys. Rev. Lett. **75**, 2638 (1995)
13. T.L. Gustavson, P. Bouyer, M.A. Kasevich, Phys. Rev. Lett. **78**, 2046 (1997)
14. Ch. Lisdat, M. Frank, H. Knöckel, M.-L. Almazor, E. Tiemann, Eur. Phys. J. D **12**, 235 (2000)
15. J.P. Toennies, private communication (2001)
16. B. Brezger, L. Hackermüller, S. Uttenthaler, J. Petschinka, M. Arndt, A. Zeilinger, Phys. Rev. Lett. **88**, 100404 (2002)
17. T. Heupel, M. Mei, M. Niering, B. Gross, M. Weitz, T.W. Hänsch, Ch.J. Bordé, Europhys. Lett. **57**, 158 (2002)
18. U. Bonse, M. Hart, Appl. Phys. Lett. **6**, 155 (1965)
19. H. Rauch, W. Treimer, U. Bonse, Phys. Lett. A **47**, 369 (1974)
20. C.R. Ekstrom, J. Schmiedmayer, M.S. Chapman, T.D. Hammond, D.E. Pritchard, Phys. Rev. A **51**, 3883 (1995)
21. T.D. Roberts, A.D. Cronin, M.V. Tiberg, D.E. Pritchard, Phys. Rev. Lett. **92**, 060405 (2004)
22. J. Schmiedmayer, M.S. Chapman, C.R. Ekstrom, T.D. Hammond, S. Wehinger, D.E. Pritchard, Phys. Rev. Lett. **74**, 1043 (1995)
23. T.D. Roberts, A.D. Cronin, D.A. Kokorowski, D.E. Pritchard, Phys. Rev. Lett. **89**, 200406 (2002)
24. J.P. Toennies, private communication (2003)
25. D.W. Keith, M.L. Shattenburg, H.I. Smith, D.E. Pritchard, Phys. Rev. Lett. **61**, 1580 (1988)
26. W. Schöllkopf, R.E. Grisenti, J.P. Toennies, Eur. Phys. J. D **28**, 125 (2004)
27. E. Arimondo, H. Lew, T. Oka, Phys. Rev. Lett. **43**, 753 (1979)
28. P.E. Moskowitz, P.L. Gould, S.R. Atlas, D.E. Pritchard, Phys. Rev. Lett. **51**, 370 (1983)
29. P.J. Martin, B.G. Oldaker, A.H. Miklich, D.E. Pritchard, Phys. Rev. Lett. **60**, 515 (1988)
30. D.M. Giltner, R.W. McGowan, Siu Au Lee, Phys. Rev. A **52**, 3966 (1995)
31. A.E.A. Koolen, G.T. Jansen, K.F.E.M. Domen, H.C.W. Beijerinck, K.A.H. van Leeuwen, Phys. Rev. A **65**, 041601(R) (2002)
32. C. Champenois, M. Büchner, R. Delhuille, R. Mathevet, C. Robilliard, C. Rizzo, J. Vigué, Eur. Phys. J. D **13**, 271 (2001)
33. C. Keller, J. Schmiedmayer, A. Zeilinger, T. Nonn, S. Dürr, G. Rempe, Appl. Phys. B **69**, 303 (1999)

34. M. Büchner, R. Delhuille, A. Miffre, C. Robilliard, J. Vigué, C. Champenois, Phys. Rev. A **68**, 013607 (2003)
35. J. Schmiedmayer, M.S. Chapman, C.R. Ekstrom, T.D. Hammond, D.A. Kokorowski, A. Lenef, R.A. Rubinstein, E.T. Smith, D.E. Pritchard, in *Atom interferometry*, edited by P.R. Berman (Academic Press, 1997), p. 1
36. J. Blanc et al., J. Chem. Phys. **96**, 1793 (1992)
37. A. Miffre, M. Jacquey, M. Büchner, G. Trénec, J. Vigué, Phys. Rev. A **70**, 030701 (R) (2004)
38. A. Miffre, M. Jacquey, M. Büchner, G. Trénec, J. Vigué, J. Chem. Phys. (`http://fr.arxiv.org/abs/physics/0406124`)
39. R. Delhuille, A. Miffre, E. Lavalette, M. Büchner, C. Rizzo, G. Trénec, J. Vigué, H.J. Loesch, J.P. Gauyacq, Rev. Sci. Instrum. **73**, 2249 (2002)
40. C. Champenois, M. Büchner, J. Vigué, Eur. Phys. J. D **5**, 363 (1999)
41. F. Biraben, P. Labastie, Opt. Commun. **41**, 49 (1982)
42. T.W. Hänsch, B. Couillaud, Opt. Commun. **35**, 441 (1980)
43. C.J. Sansonetti, B. Richou, R. Engleman Jr, L.J. Radziemski, Phys. Rev. A **52**, 2682 (1995)
44. W. McAlexander, E. Abraham, R. Hulet, Phys. Rev. A **54**, R5 (1996)
45. K. Hornberger, S. Uttenthaler, B. Brezger, L. Hackermüller, M. Arndt, A. Zeilinger, Phys. Rev. Lett. **90**, 160401 (2003)
46. K. Hornberger, J.E. Sipe, Phys. Rev. A **68**, 012105 (2003)
47. L. Hackermüller, K. Hornberger, B. Brezger, A. Zeilinger, M. Arndt, Appl. Phys. B **77**, 781 (2003)
48. Q.A. Turchette, D.E. Pritchard, D.W. Keith, J. Opt. Soc. Am. A **9**, 1601 (1992)
49. R. Delhuille, A. Miffre, B. Viaris de Lesegno, M. Büchner, C. Rizzo, G. Trénec, J. Vigué, Acta Phys. Pol. **33**, 2157 (2002)
50. N.F. Ramsey, *Molecular beams* (Oxford University Press, 1956), p. 16
51. J. Schmiedmayer, C.R. Ekstrom, M.S. Chapman, T.D. Hammond, D.E. Pritchard, J. Phys. II France **4**, 2029 (1994)
52. D.M. Giltner, Ph.D. thesis, Colorado State University, Fort Collins (1996)